

**QUANTIFYING SOURCE EXCITATION AND PATH EFFECTS FOR HIGH FREQUENCY REGIONAL WAVES**

Ru-Shan Wu, Xiao-Bi Xie, Zengxi Ge, Xianyun Wu, and Thorne Lay

University of California, Santa Cruz

Sponsored by Air Force Research Laboratory

Contract No. DTRA01-01-C-0076

**ABSTRACT**

A finite-difference modeling plus slowness analysis method is developed for predicting the Lg-wave energy. The method allows us to investigate near source energy partitioning in multiple domains including frequency, slowness and time. The main advantage of this method is that it can be applied at close range, well before Lg is actually formed at larger distance. To test the method, a large model is used in the calculation. The short distance array measurements can be directly compared with the long distance surface measurements. The two types of results show the consistency that verifies the validity of the analysis method.

We have extended the boundary element method from 2D SH case to the P-SV case. The method allows us to accurately handle the wave propagation in models with irregular topography. The validity and accuracy of the method have been checked by comparing the results with other numerical results. We also developed a connecting technique to reduce the cost of the boundary element method when calculating long distance forward propagations. Although the boundary element method is less efficient, it provides an accurate solution that can be used to calibrate other fast numerical methods with approximations. We also used the boundary element method to investigate the effect of the near source topography on the Rg-Lg coupling.

The half-space screen method has been further improved to model Lg-wave propagation in the complex crustal waveguides. Many crustal waveguide characteristics that potentially contribute to the Lg-wave attenuation have been built into the propagator. Results from the propagator provides a useful tool for investigating the relationship between the Lg wave attenuation and crustal waveguide properties. The half-space screen method has been extended to the P-SV case including the Rayleigh wave. Preliminary results are obtained and compared to the 2D elastic finite-different result.

## **OBJECTIVE**

The regional seismic phase Lg is one of the most useful phases for event discrimination and magnitude estimation associated with monitoring a CTBT. The characteristics of Lg are strongly affected by the excitation conditions in the source region and by path effects controlled by waveguide structures of different scales. To obtain a comprehensive understanding of Lg signals, it is crucial to do research on both the excitation and propagation of Lg for realistic crustal models. The Regional Wave Synthetic Seismogram program, a branch of the Institute of Geophysics and Planetary Physics (IGPP) at the University of California, Santa Cruz (UCSC) has done extensive work on the excitation and propagation of regional phases, and has developed the theory and methods for the investigation of these problems.

Currently, there are three research directions under this project. (i) A finite-difference modeling plus slowness analysis method developed for predicting the Lg-wave energy development. This method allows us to investigate near source energy partitioning in the multiple domains including frequency, slowness, and time. The main advantage of this method is that it can be applied at a close range, which is well before the Lg is actually formed at greater distance. This year we used a larger crustal model in the calculation. The short distance array measurements are directly compared with the long distance surface measurements. The two types of results show consistency that verifies the validity of the analysis method. (ii) We extended the boundary element method from 2D SH case to the P-SV case. The accuracy of the method has been carefully checked. Although the boundary element method is not an efficient solution, it provides a flexible and accurate way to solve the wave propagation problems in crustal models with irregular free surfaces. There are two motivations to introduce the boundary element method into the Lg wave analysis. First, we need an accurate solution to calibrate other fast approximations. Second, we will use the boundary element method to investigate the effect of near source topography on the couplings between the Pg, Rg and Lg waves. (iii) We are continually working on the high efficiency generalized screen propagator (GSP) for Lg propagation (Wu et al., 2000a,b; Wu and Wu, 2001). This year we applied the elastic screen propagator to investigate the Lg wave path effects. More realistic crustal models including the heterogeneities of different scales and intrinsic attenuations are being used in the numerical simulation. At the same time, we are working on the coupling issues between the body waves and the surface waves for the P-SV propagator.

## **RESEARCH ACCOMPLISHED**

### **Rg-Lg Coupling, Pg-Lg Coupling and the Lg-Wave Energy Partitioning**

Lg is predominantly comprised of shear wave energy trapped in the crust. Explosions are not efficient sources to generate shear energy. Although several mechanisms have been proposed to convert P-wave energy into Lg waves, e.g., spall, tectonic release, S\*-wave, free surface reflection pS, etc., they often require certain environmental conditions that do not exist. Compared to deeper earthquake sources, shallow explosions generate relatively large Rg phases, which is readily disrupted by crustal heterogeneities. Rg energy may scatter into trapped crustal S-waves near the source region and contribute to a low-frequency Lg-wave (Gupta et al., 1991, 1992). In this project we develop a method, based on the finite-difference simulation and slowness analysis, to investigate the contributions of Rg-Lg and Pg-Lg couplings relative to the explosion of energy partitioning. To investigate these mechanisms it requires very fine near source velocity models, however in order to obtain well-developed Lg phases, the waves need be propagated up to very long distances. To overcome this difficulty, Xie and Lay (1994) proposed a slowness analysis method. With this method, fine velocity structures are used in the near source region, which provide coupling conditions between Pg, Rg and Lg waves. The finite-difference method is used to propagate the seismic waves in the crustal waveguide. In the intermediate distances, energy flux in the waveguide is calculated from synthetic seismograms using the array technique. The energy that will contribute to the Lg wave can be measured and used as an indicator of Lg wave energy at a longer distance. The slowness analysis can be conducted well before the Lg-wave is fully formed. The entire system requires only a compact sized model and it provides an efficient tool for investigating different near source Lg-wave excitation mechanisms.

In the previous year, we tested this method and obtained some preliminary results. Further simulations are being conducted this year. Figure 1 shows the configuration of the model used to calculate the Lg wave propagation. The explosion source is located at a depth of 750 m. A 2D elastic finite-difference code (Xie and Lay, 1994) is used to generate the synthetic seismograms. A Gaussian derivative source time function is used and the effective frequency band is roughly 0 to 5 Hz.

Synthetic seismograms are collected from two receiver arrays for different investigations. The first is a 50x40 array with 1 km spacing located 150 km from the epicenter and is used for short distance slowness analysis. The second receiver array is located on the surface, 450 km from the epicenter, which simulates conventional Lg wave observations. The energy partitioning obtained from the shorter distance is compared to the surface Lg observations at the longer distance.

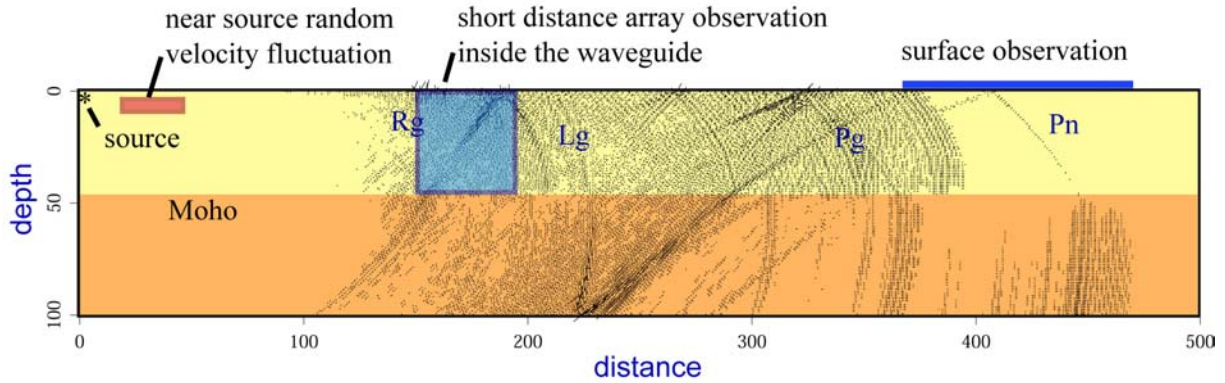


**Figure 1. Cartoon showing the process of FD simulation and slowness analysis. The FD method is used to generate synthetic seismograms within the crustal waveguide. Near source random velocity fluctuations are added to the background velocity to generate Pg to Lg and Rg to Lg couplings. Energy flux at a short distance is calculated using an array technique then analyzed based on the slowness, frequency, and travel-times. The energy that will contribute to the Lg can be measured and used as an indicator of Lg wave energy at a longer distance.**

We use a layered velocity structure that resembles the east Kazakh crust as the background model. This is a typical high-velocity crust where the upper crust P-wave velocity is larger than the upper mantle S-wave velocity. For such a velocity structure, very little energy generated from an explosion source can be trapped in the waveguide to form the Lg-wave. To investigate the near source Rg to Lg and Pg to Lg couplings, we add some small random velocity patches near the source region. These random patches are 10 km wide, 2.5 km thick, located at the epicenter a distance of 5-15 km and at different depths. The RMS velocity fluctuation for these patches is 10 % with a 1 km correlation length for both vertical and horizontal directions. Synthetic seismograms computed at the receiver arrays are used for the slowness analysis. The size of the sub-array for slowness analysis is 10x10.

Figure 2 shows the slowness analysis results at 180 km in the crustal waveguide. The data is processed in three frequency bands. The left, middle and right columns are for 0.3-1.5 Hz, 0.8-2.0 Hz and 2.0-5.0 Hz pass bands, respectively. In each panel, the vertical axis is the horizontal phase velocity. The horizontal axis is time. The group velocity is also marked on the top of each panel. The dashed line marks the upper mantle S-wave velocity. The solid circles are energy picked from the slowness domain and summed up for the entire cross section. The top row is for the background velocity model. Little Lg energy can be observed, which is typical for such a high velocity crustal waveguide. The following rows are for crust models with near source random velocity perturbations. We first focus on the low frequency results (left panel). From the top panel we can see a strong Rg-wave. However, there is little energy within the Lg wave window. In the second panel, a random velocity patch located at a depth of 0.0-2.5 km is added to the background model. Compared with the background model, considerable energy is transferred from the Rg-wave to the Lg-wave through scattering. Panels 3 to 5 are similar to panel 2, except that random patches are located at depths of 2.5-5.0 km, 5.0-7.5 km, and 10.0-12.5 km, respectively. Similar to the case in the second panel, energy is transferred from Rg to Lg. The tendency is: the shallower the random patch the more energy is scattered from Rg to Lg. This also provides additional evidence that the low frequency Lg energy comes from the Rg-wave, since the Rg energy is mostly concentrated at the shallow depth.

In the high frequency results (right panel), from the top panel we can see a strong Pg-wave. There is some energy fall into the Lg group velocity window. However, these energy have a high horizontal phase velocity implying they are coming from Pg-wave through Pg to Sg reflections on a flat free surface or Moho discontinuity. As a result of the steep incident angles the energy will gradually leak to the upper mantle and cannot form the Lg-wave. In the

following panels, after adding random velocity perturbations in the near source region, part of the Pg energy transfer to the Lg window, i.e., scattered energy falls into the proper slowness window. In general, the Rg-Lg coupling takes place at a lower frequency and the Pg-Lg coupling at a higher frequency.

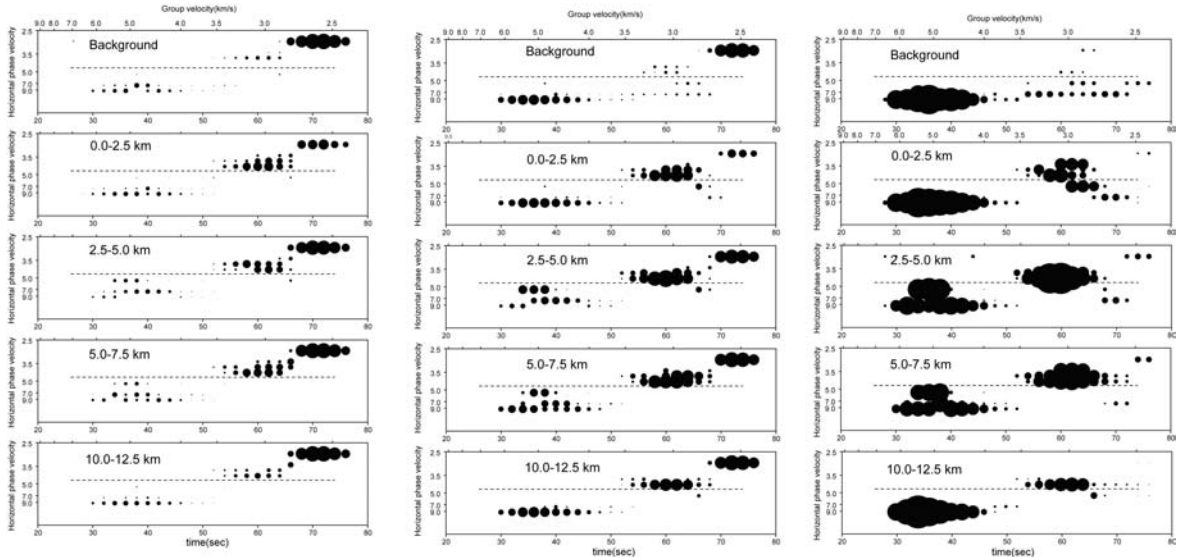


Figure 2. Examples of slowness analysis. From left to right are for 0.3-1.5 Hz, 0.8-2.0 Hz, and 2.0-5.0 Hz frequency bands. The top row is for the background velocity model without any randomness, and the following rows are for models with random patches at different depths. Random velocity patches extend from a distance of 5-15 km and are located at depths from 0 to 15 km.

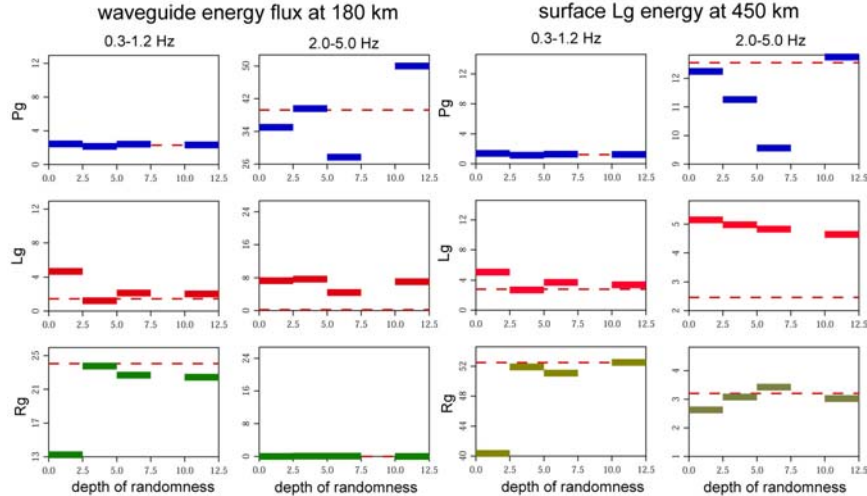
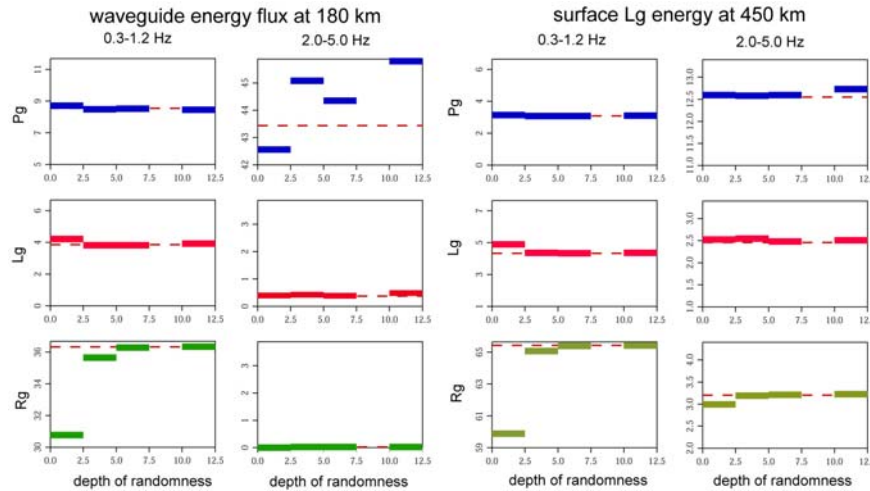


Figure 3. Comparison between the waveguide energy flux at 180 km (left two panels) and the wave energy on the surface at 450 km (right two panels). Shown in each small panel is relative energy, the horizontal axis is the depth of the random patches, and the vertical axis is the energy. Dashed line indicates the energy level for the background velocity model. Short bars indicate the energy changes as a result of the random velocity fluctuations.

The two left columns in Figure 3 give the relationships between the energy of different wave types and the depth of the random velocity perturbations. Column 1 is for low frequency and column 2 is for high frequency. As comparisons, the two right columns (3 and 4) give the energy from the surface array at a distance of 450 km from the epicenter. The surface observations are obtained by calculating the RMS amplitudes in different group velocity windows, which is similar to the conventional Lg-wave observations. The relative energy is shown in each small

panel. The horizontal axis is the depth of the random patches, and the vertical axis is the energy. The dashed line indicates the energy level for the background velocity model. The short bars indicate the energy changes due to the random velocity fluctuations. By comparing columns 1 and 3, we see that at a lower frequency, energy exchange mainly occurs between the Rg and Lg waves. There is almost no Pg energy. Since Rg energy is more concentrated in the shallow depth, the Rg-Lg coupling is more sensitive to the shallow velocity perturbations. The slowness analysis at a short epicenter distance correctly predicts the Lg surface wave energy observed at a greater distance. By comparing columns 2 and 4, we see that at a higher frequency, energy exchange occurs between the Pg and Lg waves. The Pg-Lg coupling is less sensitive to the depth of the randomness. For Lg waves, the slowness analysis result is consistent with the surface Lg observation at the greater distance. For Pg waves, there is a discrepancy between the two measurements. Since the Pg-wave is not a trapped wave, the result suggests that part of the Pg energy leaks to the upper mantle before it reaches the greater distance. These comparisons verify that the current analysis method can be used to investigate the near source Lg excitation and energy partitioning mechanisms such as Pg-Lg and Rg-Lg couplings.



**Figure 4. Comparison between waveguide energy flux at 180 km (left panel) and the wave energy on the free surface at 450 km (right panel). This figure is similar to the Figure 3, except the random velocity patches are located between 45 km and 55 km. Because the random patches are located farther away from the source, the coupling between the Rg and Lg is weaker.**

Figure 4 is similar to the Figure 3, except that the random velocity perturbations are between 45 km and 55 km from the epicenter. Once again, the low frequency energy flux at a shorter distance correctly predicts the surface Lg wave observations at a larger distance. Because the random velocity perturbations are located farther away from the source, the coupling between the Rg and Lg waves are weaker compared to the near source velocity perturbations. However, if there are velocity perturbations along the entire propagation path, their accumulated effects may still generate considerable Lg energy.

### **Boundary Element Modeling of P-SV Wave Scattering from the Irregular Topography**

#### **Summary of the boundary element method**

The Lg wave is composed of multiple reflected shear waves between the free surface and the MOHO discontinuity. Surface topography has an important effect on the Lg-wave excitation and propagation. Although the boundary element method is not an efficient method, it provides a flexible and accurate solution for wave propagation in the models with irregular free surfaces. There are two goals of introducing the boundary element method in the Lg wave analysis. First, we will use an accurate boundary element result to calibrate other fast approximations. Second, we will use the boundary element method to investigate the effect of near source topography on the coupling between the Pg, Rg, and Lg waves. Fu and Wu (2001) applied the boundary element method for calculating the SH-wave propagation. We extend the frequency-domain direct boundary element method to the P-SV case for models with irregular topographies.

Considering the 2-D P-SV wave propagation in a homogeneous region  $V$  bounded by surface  $S$ , the displacement  $\mathbf{u}(\mathbf{r})$  at location  $\mathbf{r}$  can be calculated by representation integrals (e.g., Aki and Richards, 1980)

$$\mathbf{C}(\mathbf{r})\mathbf{u}(\mathbf{r}) + \int_S \boldsymbol{\Sigma}(\mathbf{r}, \mathbf{r}')\mathbf{u}(\mathbf{r}')dS = \int_S \mathbf{G}(\mathbf{r}, \mathbf{r}')\mathbf{t}(\mathbf{r}')dS + \int_V \mathbf{G}(\mathbf{r}, \mathbf{r}')\mathbf{f}(\mathbf{r}')dV \quad (1)$$

where  $\mathbf{f}$  is the body force,  $\mathbf{G}(\mathbf{r}, \mathbf{r}')$  and  $\boldsymbol{\Sigma}(\mathbf{r}, \mathbf{r}')$  are Green's functions of the displacement and traction,  $\mathbf{t}(\mathbf{r})$  is the traction,  $\mathbf{C}(\mathbf{r})$  is the coefficient matrix, which can be expressed as

$$\mathbf{C}(\mathbf{r}) = \begin{cases} \mathbf{I} & \mathbf{r} \in V \\ \dot{\mathbf{C}}(\mathbf{r}) & \mathbf{r} \in S \\ \mathbf{0} & \mathbf{r} \notin V \end{cases} \quad (2)$$

and

$$\dot{\mathbf{C}}(\mathbf{r}) = \frac{1}{4\pi(1+\mu)} \begin{pmatrix} 2(1-\nu)(\theta_1 - \theta_2) + \frac{1}{2}(\sin 2\theta_1 - \sin 2\theta_2) & (\sin^2 \theta_1 - \sin^2 \theta_2) \\ (\sin^2 \theta_1 - \sin^2 \theta_2) & 2(1-\nu)(\theta_1 - \theta_2) - \frac{1}{2}(\sin 2\theta_1 - \sin 2\theta_2) \end{pmatrix} \quad (3)$$

where  $\mu$  is the shear module and  $\nu$  is the Poisson's ratio. Note that the matrix  $\dot{\mathbf{C}}$  depends on  $\theta_1$ ,  $\theta_2$  and the orientation of the side of the angle in the global coordinate. For simplicity, let  $\mathbf{r}' = \mathbf{0}$ . In an unbounded homogeneous isotropic elastic medium, the Green's functions for 2-D P-SV case can be expressed as

$$G_{ij}(\mathbf{r}) = \frac{1}{2\pi\rho\beta^2} [\psi\delta_{ij} - \phi r_{,i}r_{,j}]$$

$$\Sigma_{ij}(\mathbf{r}) = \frac{1}{2\pi} \left[ \left( \frac{\partial\psi}{\partial r} - \frac{\phi}{r} \right) (\delta_{ij}r_{,k}n_k + r_{,j}n_i) - \frac{2\phi}{r} (r_{,i}n_j - r_{,i}r_{,j}r_{,k}n_k) \right]$$

$$- 2 \frac{\partial\phi}{\partial r} r_{,i}r_{,j}r_{,k}n_k + \left( \frac{\alpha^2}{\beta^2} - 2 \right) \left( \frac{\partial\psi}{\partial r} - \frac{\partial\phi}{\partial r} - \frac{\phi}{r} \right) r_{,i}n_j$$

where  $r = |\mathbf{r}|$ ,  $\mathbf{n}$  is the normal vector of  $S$  and pointing outside. “ $i$ ” and “ $j$ ” denote  $\partial/\partial x_i$  and  $\partial/\partial x_j$ ,  $\alpha$  and  $\beta$  are P- and S-wave velocities, and

$$\psi = \frac{i\pi}{2} \left[ H_0^{(1)}(k_s r) - \frac{1}{\beta r} \left( H_1^{(1)}(k_s r) - \frac{\beta}{\alpha} H_1^{(1)}(k_p r) \right) \right]$$

$$\phi = \frac{i\pi}{2} \left[ \frac{\beta^2}{\alpha^2} H_1^{(1)}(k_p r) - H_1^{(1)}(k_s r) \right]$$

where  $H^{(1)}(\cdot)$  is the Hankel function of the first kind,  $k_p$  and  $k_s$  are P and S wavenumbers, respectively. In the frequency-domain, equation (1) can be discretized along the boundary  $S$ , which may include irregular topography. Assuming  $\mathbf{u}(\mathbf{r})$  and  $\mathbf{t}(\mathbf{r})$  are located on the surface  $S$  and linear over each of the  $N$  boundary elements, we have the system of linear equations

$$\mathbf{C}(\mathbf{r}^l)\mathbf{u}(\mathbf{r}^l) + \sum_{m=1}^N \left\{ \left[ \boldsymbol{\Sigma}(\mathbf{r}^l, \mathbf{r}^m)\mathbf{u}(\mathbf{r}^m) \right] - \left[ \mathbf{G}(\mathbf{r}^l, \mathbf{r}^m)\mathbf{t}(\mathbf{r}^m) \right] \right\} = \mathbf{u}^0(\mathbf{r}^l) \quad (4)$$

Here  $l$  and  $m$  denote the indexes of elements. For free surface,  $\mathbf{t}(\mathbf{r}) = \mathbf{0}$ . For internal interfaces, continuity conditions of displacements and stresses should be satisfied. By solving the linear equations, the displacements and stresses at all boundary elements can be obtained. Using the integral representation, the wavefield everywhere inside the volume can then be obtained.

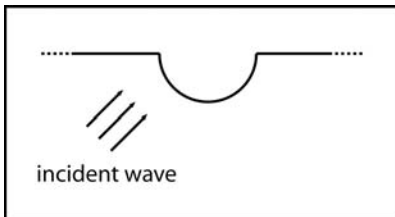
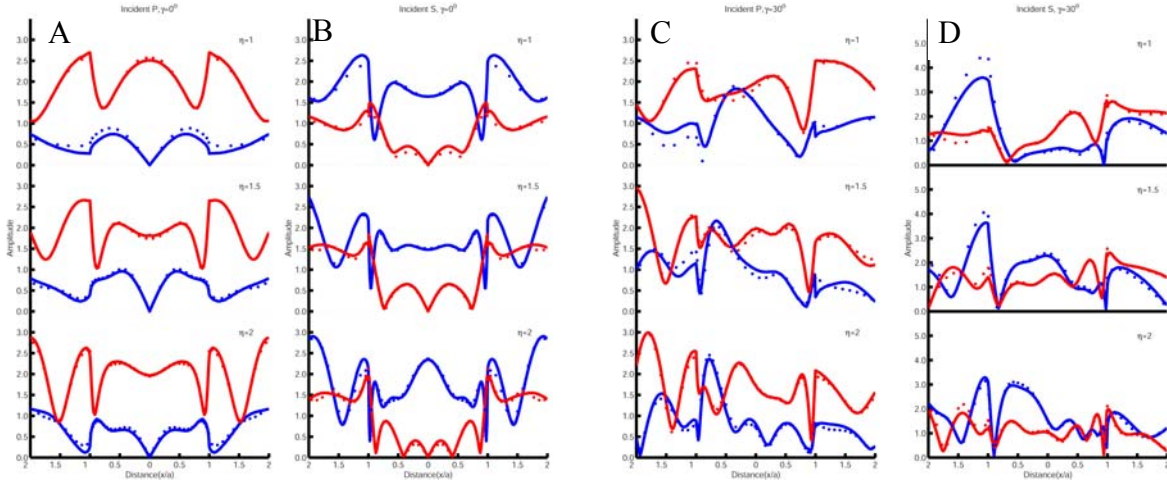


Figure 5. A semicircular canyon model.

**Numerical tests.** To test the accuracy of the method, we conducted a series of calculations using our boundary element method and compared the results with those calculated from other methods. The first model is a semicircular canyon on a homogeneous half-space with a Poisson's ratio of 1/3 (Figure 5). The plane waves with incident angles of 0 degree and 30 degrees are incident on the free surface. This problem has been studied by many authors for

example: Kawase, 1988; Sanchez-Sesma and Rosenbluth, 1979; and Sanchez-Sesma and Campillo, 1991. Their results were in agreement with each other. Here we compare our results to that of Sanchez-Sesma and Campillo (1991) and calculated them using an indirect boundary integral method. The results of plane P and SV waves with incident angles 0 and 30 degrees are shown in Figure 6. Normalized frequencies  $\eta = \omega a / \pi \beta = 1.0, 1.5,$  and  $2.0$  are used in the calculation. The results show good agreement with the previous authors.



**Figure 6.** The comparison between our results and Sanchez-Sesma's results for a semicircular canyon model. **A:** vertical P-wave incidence, **B:** vertical SV-wave incidence, **C:** 30 degree P-wave incidence and **D:** 30 degree SV-wave incidence. From upper to bottom are for normalized frequencies 1.0, 1.5 and 2.0. The solid lines denote our results and the dotted lines denote Sanchez-Sesma's results.

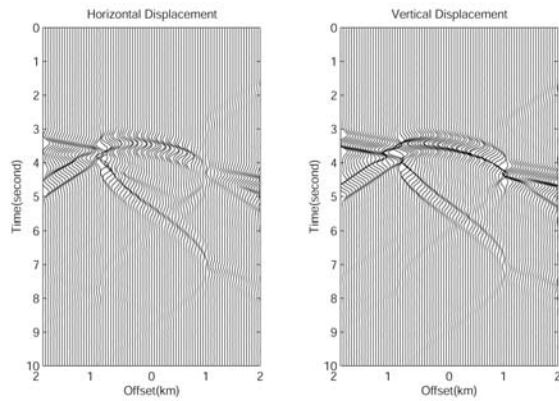


**Figure 7.** Synthetic seismograms at the free surface of a semicircular canyon. A 30 degree P-wave is incident on the surface. On the left and right are horizontal and vertical components.

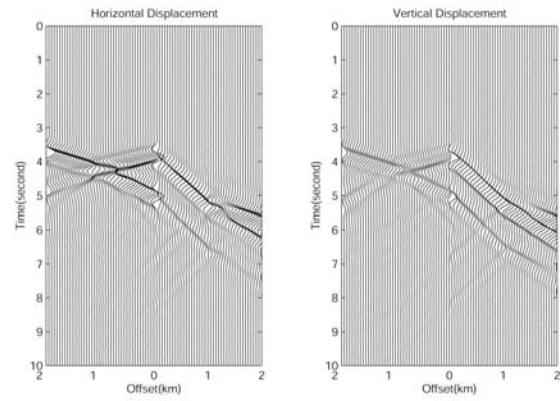


**Figure 8.** Synthetic seismograms at the free surface of a triangular canyon. A 30 degree SV-wave is incident on the surface. On the left and right are horizontal and vertical components.

Shown in Figure 7 are synthetic seismograms on the free surface of a semicircular canyon. A 30 degree P-wave is incident on the surface. The receivers are located along the surface from -2 to 2 km. The reflected P-wave can be clearly seen along the left wall of the canyon. We can also see the creeping Rayleigh waves that propagate along the surface of the canyon. Similarly, Figure 8 shows the response of a triangular canyon to a 30 degree SV-wave incidence. Reflected P waves and diffracted Rayleigh waves from the edges of the canyon can be identified in the synthetic seismograms.

To reduce the computation cost, especially for long propagation distances, we designed a connection technique. To avoid solving a huge matrix, the entire waveguide is divided into several sections. Artificial interfaces are

introduced between the adjacent sections. Assuming that the Lg wave does not produce multiple scattering between different sections, a transparent boundary condition can be adopted at these artificial boundaries. The output from one section can be used as the input of the next section. The entire matrix can be divided into several small matrixes and fit into conventional computer memories. Figure 9 gives a simple example on how this technique works. The waveguide is composed of a flat one-layer crust over the upper mantle. The solid lines are synthetic seismograms calculated directly from the source to the receivers. The dotted lines are synthetic seismograms calculated using the connection technique. The two results are consistent with each other.

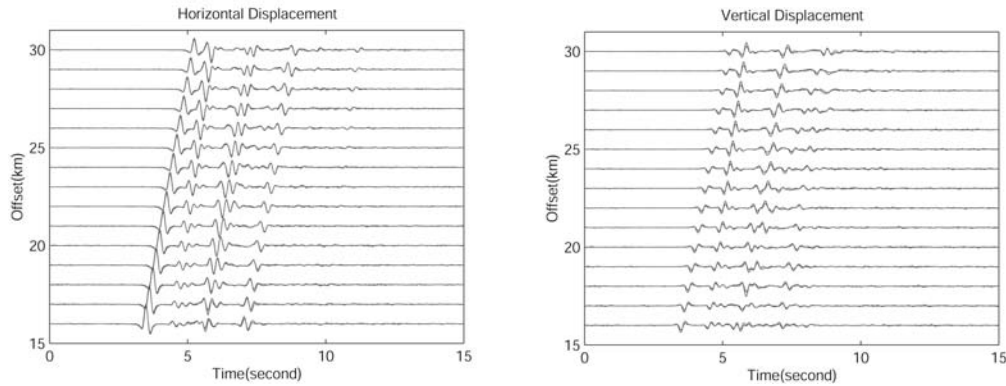


**Figure 9.** Comparison of synthetic seismograms calculated using the connection technique (dotted lines) and those directly calculated from the source to receivers (Solid lines). On the left is the horizontal component and on the right is the vertical component.

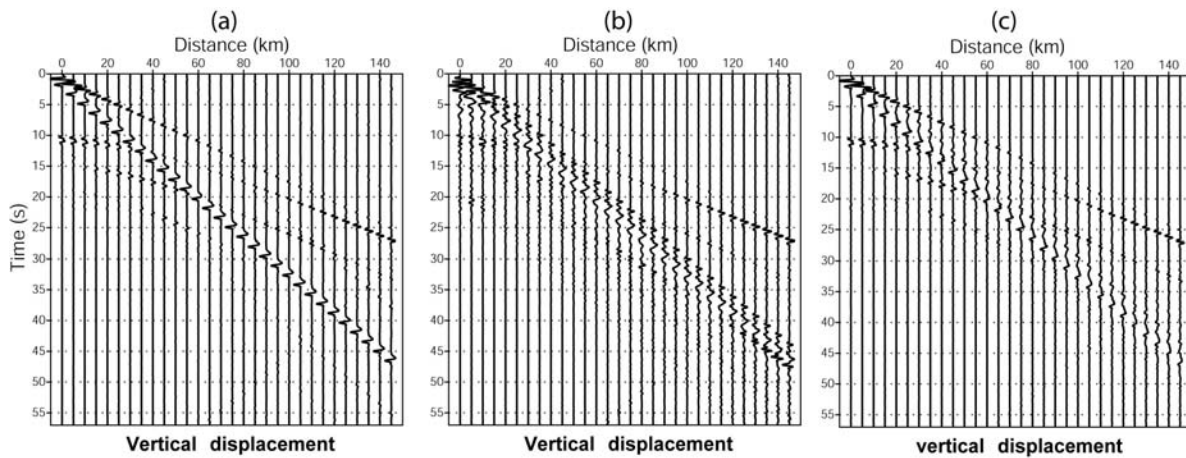


**Figure 10.** Scattering of Rg waves due to irregular free surface: (a) reference model with a flat free surface, (b) model with a near source irregular free surface, and (c) model with mild irregular free surface along the entire path.

### Rg wave scattering on the irregular topography

To investigate the effect of irregular topography on the Rg scattering, we calculated the synthetic seismograms for crustal waveguide models with and without irregular topographies. In Figure 10 we show the vertical component of a synthetic seismograms for different velocity models. Figure 10a is the reference model, which is a two-layer model composed of a flat crust and a homogeneous upper mantle. The depth of the Moho discontinuity is 32 km. The P- and S-wave velocities for the crust are 6 km/s and 3.4 km/s, and 8.0 km/s and 4.6 km/s, respectively, for the upper mantle. In Figure 10b, a section of a near source irregular topography is added to the reference model between 0 and 20 km. Its RMS value is 0.6 km and the correlation length is 1 km. In Figure 10c, the model has an irregular topography along the entire free surface. Its RMS value is 0.3 km and the correlation length is 5 km. Both irregular topographies provide the Rg-wave scatterings although their appearances are different. Detailed characteristics of

these scatterings and their contributions to the explosion source energy partitioning will be investigated in the future.

### **Simulation of Lg Wave Propagation and Blockage Using the Elastic Screen Method**

Many observations reveal that the attenuation of the regional phase Lg relates to the waveguide structures of all scales. Both elastic and anelastic properties contribute to the attenuation. However, the mechanism of the Lg wave attenuation has not been fully understood. The numerical simulation is still one of the most important ways to investigate the Lg wave attenuation mechanisms. We continue to investigate the path effects using the elastic screen propagators. More realistic crustal models including heterogeneities of different scales and intrinsic attenuations are used in the numerical simulations. Two numerical examples are presented here to show how this method works.

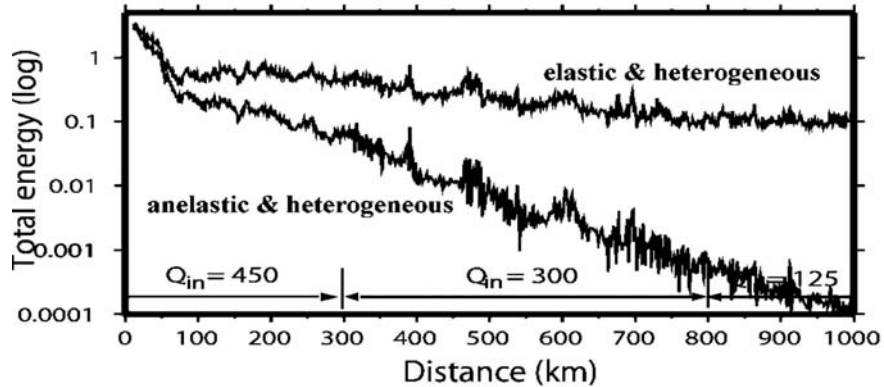


**Figure 11. Synthetic SH Lg wave attenuation curves for Tibetan Plateau. Compared to the elastic case, the anelastic crust gives much higher Lg energy attenuation.**

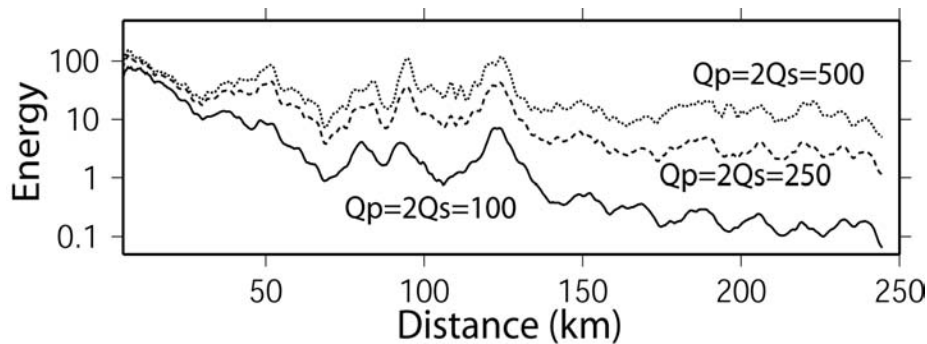


**Figure 12. Synthetic P-SV Lg wave attenuation curves for the Flora-Asnes crust model. The intrinsic attenuation in the crust plays an important role for Lg energy attenuation.**

### **SH Lg simulation for the Tibetan Plateau model.**

Regional phase Lg has been widely observed across Asia. However, for the propagation paths crossing the Tibetan Plateau, little energy can be observed. It has been demonstrated that the Lg-wave undergoes an abnormally strong attenuation in this region. For the SH case, a waveguide model based on the actual topography and the depth of the Moho discontinuity is designed for the simulation. In addition to the large-scale crustal structures, random velocity fluctuation is added to the crustal waveguide. The horizontal and vertical correlation lengths of the random fluctuation are 10 km and 5 km. The RMS velocity perturbation is 10%. The source is located at a depth of 16 km and its dominant frequency is 2 Hz. Both elastic and anelastic models are used in the calculation. For the anelastic case, a laterally varying intrinsic attenuation is added to the model. Figure 11 gives the Lg energy attenuation curves along a 1000 km path. Even with the proper heterogeneities, the elastic model fails to explain the observed strong Lg attenuation and its regional distribution. On the other hand, after the intrinsic attenuation is introduced, the Lg energy dropped three orders of magnitude compared with the elastic model. The results are compatible with the observations in the region.

### **P-SV Lg-wave propagation in the Flora-Asnes crust model**

For the P-SV wave case, we are continually working to improve the stability of our complex screen propagator for long distance propagation. At the same time, we are working on the couplings between the body waves and the surface wave. Figure 12 shows the P-SV Lg wave attenuation versus distance. The 1-D background model is the Flora-Asnes crust model in the NORSAR region. A random velocity fluctuation with a 10% RMS value and correlation lengths similar to the SH wave case is added to the background model. Three sets of P- and S-wave quality factors are used in the calculation. The results show that the intrinsic attenuation plays an important role in the Lg wave energy decay.

### **CONCLUSIONS AND RECOMMENDATIONS**

The purpose of the project is to develop computationally viable techniques for investigating the excitation and path effects of high frequency regional waves. Currently there are three research directions under this project. First, a finite-difference modeling plus slowness analysis method is developed for predicting the Lg-wave energy. This work is essential for both discriminating explosions and earthquakes, and for understanding Lg wave energy partitioning. Second, the boundary element method for both SH and P-SV cases are developed and tested. Although the boundary element method is not an efficient solution, we can use it to calibrate other fast approximations and investigate the effect of near source topography on the Rg-Lg coupling. Third, We are continually working on the high efficiency GSP propagators for both SH and P-SV Lg-wave simulations. In general, we are trying to build computational tools that can handle more realistic crust models and use these tools to investigate the excitation and propagation of Lg-waves in different geological structures.

### **REFERENCES**

- Aki, K. and P.G., Richard (1980), Quantitative seismology, W. H. Freeman, San Francisco.
- Fu, L.Y. and R.S., Wu (2001), A hybrid BE-GS method for modeling regional wave propagation, *Pure and Apply Geophysics*, 158, 1251-1277.
- Gupta, I.N., W.W. Chan, and R.A. Wagner (1992), A comparison of regional phases from underground nuclear explosions at east Kazakh and Nevada test sites, *Bull. Seism. Soc. Am.*, 82, 352-382.
- Gupta, I.N., T.W. McElfresh, and R.A. Wagner (1991), Near source scattering of Rayleigh to P in teleseismic arrivals from Pahute Mesa (NTS) shots, in *Explosion Source Phenomenology*, edited by, Taylor, S.R., Patton, H.J. and Richards, P.G., American Geophysical Union, Washington, DC.
- Kawase, H. (1988), Time domain response of a semicircular canyon for incident SV, P, and Rayleigh waves calculated by the discrete wavenumber boundary element method, *Bull. Seism. Soc. Am.* 78, 1415-1437.
- Sanchez-Sesma, F.J. and M., Campillo (1991), Diffraction of P, SV and Rayleigh waves by topographic features: A boundary integral formulation, *Bull. Seism. Soc. Am.*, 81, 2234-2253.
- Sanchez-Sesma, F. J. and E., Rosenblueth (1979), Ground motion at canyons of arbitrary shape under incident SH waves, *Intl. J. Earthq. Eng. Struct. Dyn.*, 7, 4441-4450.
- Wu, R.S., S. Jin, X.B. Xie (2000a), Seismic wave propagation and scattering in heterogeneous crustal waveguides using screen propagators: I SH waves, *Bull. Seis. Soc. Am.*, 90, 401-413.
- Wu, R.S., S. Jin, X.B. Xie (2000b), Energy partition and attenuation of Lg waves by numerical simulations using screen propagators, *Phys. Earth and Planet. Inter.*, 120, 227-244.
- Wu, X.Y. and R.S. Wu (2001), Lg-wave simulation in heterogeneous waveguides with surface topography using screen propagators, *Geophys. J. Int.*, 146, 670-678.
- Xie, X.B. and T. Lay (1994), The excitation of Lg waves by explosions: A finite-difference investigation, *Bull. Seism. Soc. Am.*, 84, 324-342.